January 10th, 2019

MS# POWER-D-18-04728 (revised)

$Cu_xCo_{3-x}O_4$ ultra-thin film as efficient anodic catalysts for anion exchange membrane water electrolysers

E. López-Fernández, [1,2] J. Gil-Rostra,[1] J. P. Espinós,[1] A. R. González-Elipe[1], F. Yubero,[1*] A. de Lucas Consuegra[2,*]

[1]Laboratory of Nanotechnology on Surfaces, Institute of Materials Science of Seville (CSIC - Univ. Sevilla), Av. Américo Vespucio 49, E-41092 Sevilla, Spain

[2]Department of Chemical Engineering, School of Chemical Sciences and Technologies, University of Castilla-La Mancha, Avda. Camilo José Cela 12, E-13071, Ciudad Real, Spain.

*Corresponding authors. E-mail address: Antonio.LConsuegra@uclm.es; Yubero@icmse.csic.es

Abstract

$Cu_xCo_{3-x}O_4$ ultra-thin films, deposited by magnetron sputtering at oblique angles have been used as anodic catalysts in anion exchange membrane water electrolysers. It has been demonstrated that the used deposition procedure provides porous and amorphous samples with a strict control of the total catalyst load and Co/Cu ratio. Electrocatalytic tests showed a maximum performance for the oxygen evolution reaction at Co/Cu atomic ratio around 1.8. The optimized anodic catalyst presented a long-term stability confirmed by accelerated lifetime tests together with the chemical surface analysis of the used samples. The effect of the crystallization of a single layer $Cu_xCo_{3-x}O_4$ and a multilayer $(CuO/Co_3O_4)^n$ anodic catalyst samples was also investigated. The loss of catalytic performance found in both cases may prove that a particular local chemical environment around the Co and Cu sites acts as an efficient catalytic site for the oxygen evolution reaction. A catalyst film with the optimum Co/Cu atomic ratio was incorporated into a Membrane Electrode Assembly, using a sputtered Ni film as cathode. Current density values up to 100 mA cm^{-2} at 2.0 V were obtained in 1.0 M KOH electrolyte. Upon normalization by the amount of catalyst, this performance is one of the highest reported in literature.

Keywords

AEM water electrolysis; magnetron sputtering; $CuO\text{-}Co_3O_4$; OER; hydrogen production

1. Introduction

Hydrogen is considered a promising energy vector in conjunction with renewable sources, although problems persist in relation to its efficient production and storage. Among the various hydrogen production methods, water electrolysis is a key sustainable and environmentally friendly process that, even if already used for industrial production, is still studied at fundamental level to improve process performance and to substitute the expensive noble metal catalysts currently used as electrodes [1-4].

There are several types of electrolysers according to their operation temperatures. Proton exchange membrane water electrolysers (PEMWE) and alkaline water electrolysers (AWE) run at low temperatures (50-80 ºC), while solid oxide steam electrolyser cells (SOEC) [5-7] operate at high temperatures (above 600-800 ºC). Although PEMWEs are energetically more efficient and have a more compact design than AWEs, they are disadvantageous due to the high cost of the available electrodes (mainly noble metal catalysts) and membranes required to operate in acid environment [5, 8]. AWEs, on the contrary, use less corrosive alkaline solutions as electrolytes, render faster kinetics and are compatible with non-noble metal catalyst electrodes [9]. However, they usually face the drawback of the formation of potassium carbonate due to carbonation of the alkaline hydroxides, mainly KOH, used as liquid electrolyte. Such a process reduces the concentration of OH^- anions in the electrolyte and therefore produces efficiency losses for the oxygen evolution reaction (OER). In addition, carbonate precipitates obstruct the pores of the gas diffusion layer producing a drop in ion conductivity and, hence, a decrease in the overall electro-catalytic activity of electrodes [2, 6].

Anion Exchange Membrane Water Electrolysis (AEMWE) would solve the problems of PEMWE and AWE technologies mentioned above. AEMWEs are compatible with non-

noble metal catalyst electrodes and can use conductivity membranes cheaper than Nafion. Besides, AEMWE incorporates anion exchange membranes making the electrolysers more compact and easier to use. Moreover, since they can operate with low alkaline concentrations or even distilled water, they can avoid the aforementioned carbonation problems [2, 5]. Clearly, increasing the catalytic performance of electrodes and finding new methods of synthesis are key issues to make AEMWE more efficient and competitive with respect to PEMWE. In fact, the catalyst incorporated in the AEMWE cell anode is of paramount importance to control the OER kinetics and, therefore, to keep low the overpotential of the cell [5, 10].

Cobalt based oxides are considered good catalysts for the OER in alkaline media because of their optimum electrochemical behavior, high electrical conductivity, high stability, low cost, and environmental compatibility [5, 10, 11]. In the quest for more efficient electrodes, it has been demonstrated that performance increases by the addition of a second element, such as Li, Ni or Cu, to form a binary mixed oxide catalyst anode [12]. In particular, previous studies with half cells have shown that the incorporation of Cu into the Co_3O_4 spinel lattice leads to more negative OER onset potentials [5].

Traditional electrode fabrication techniques of catalyst layers for this type of electrolysers consist of dripping a catalyst ink onto a porous electrode support (usually carbon paper) [5, 9, 13]. This method makes use of catalyst powders, usually prepared by thermal decomposition of precipitated metal precursors salts, gives rise to inhomogeneous electrodes with high metal loadings in the range of few or even tens of mg cm^{-2} [1, 14]. Additionally, the low reproducibility of this kind of preparation techniques hinders their straightforward scaling to stack configuration and larger areas.

Physical vapour deposition by magnetron sputtering (MS) could be a feasible way to solve some of these limitations. In the MS technique typically, a RF or pulsed DC negative voltage is applied to a target source material at low-pressure conditions (~10^{-2} mbar) causing a plasma to glow and positive ion bombardment of the target. This ion bombardment induces the ejection of material from the target onto a substrate located nearby. MS deposition gives rise to homogeneous films of controlled low metal loading and thickness, operates at room temperature, and it is easily scalable and quite reproducible [15-19]. The compactness of the deposited material with this technique can be tuned through deposition geometry, i.e., angle between the flux of sputtered particles from the target and substrate normal [19]. Thus, MS at oblique deposition angles (MS-OAD) renders mesoporous films with open microstructure (compared with normal deposition configuration that gives in general compact thin films [18]). Thus, MS-OAD may lead to produce electrodes with enhanced electrocatalytic activity in water electrolysis [15, 18, 20].

In the present work, copper-cobalt mixed oxides anodic films have been prepared for the first time in literature by a kind of MS-OAD method, characterized by different techniques and tested as OER catalysts. They have been also incorporated into a membrane electrode assembly (MEA) and tested in an electrolysis cell. The high performance found for these electrodes, in terms of current density vs. catalyst load, and their long term stability and reproducibility, support the high potential of the MS-OAD technique for the preparation of a new generation of highly reliable AEMWE electrodes. In addition, a careful characterization of these catalyst films before and after their use as anodic electrodes has provided interesting clues about the nature of the most active catalytic sites for the OER.

2. Experimental

2.1. Preparation of AEMWE electrodes

$Cu_xCo_{3-x}O_4$ mixed oxide films were prepared at room temperature by co-deposition of the two metallic cations by reactive magnetron sputtering. Pure Cu and Co targets of 50 mm diameter (GoodFellow, 99.9%) were used as metallic sources in an O_2/Ar discharge prepared with mass flow controllers set at 15 sccm for both gases.

The deposition geometry, schematized in the supporting information Figure S1, was as follows: several substrates were placed in a rotating sample holder of 10 cm diameter. The Cu magnetron head facing the substrates (normal deposition geometry) was aligned with the rotation axis of the sample holder and separated ~19 cm from it. The Co magnetron head was placed perpendicular to the plane holder plate (i.e., in an oblique deposition geometry) at a distance to the edge of the rotatable holder of ~7 cm (average deposition angle of ~70º). During the deposition process, the sample holder was continuously rotating at a rate of 5 turns per minute to homogenize the deposits.

The Co target was operated by a pulsed DC power supply (AE Pinnacle+) fixed at 150 W and a frequency of 120 kHz. The Cu target was operated with a RF power supply (RF Product, AJA 600) set between 50 and 200 W to vary the amount of deposited copper within the deposited mixed oxide. The base pressure of the system was $2 \cdot 10^{-6}$ mbar and the deposition pressure $5 \cdot 10^{-3}$ mbar. Under these conditions, the overall deposition rate varies between 4.4 and 7.7 nm min^{-1}, depending on the actual power applied to the copper target.

Pieces of polished silicon wafers, fused silica, and ITO glass panes were used as substrates for film characterization [17]. Besides, carbon paper [3] was used for electrochemical tests. The deposition process took place simultaneously in all substrates

for each experimental condition considered. We dub *equivalent thickness* the thickness of thin films deposited on the flat substrates.

To study the effect of catalyst crystallization, selected samples were annealed in air up to 500 ºC, at a rate of 5 ºC min^{-1} and maintained for 2 hours at this temperature.

Besides homogenous $Cu_xCo_{3-x}O_4$ catalyst films, $(CuO/Co_3O_4)^{10}$ multilayered samples were prepared by sequential deposition of the single oxides with the same process parameters than for the mixed oxides fixed 150 W applied to the target. The first deposited layer was CuO followed by Co_3O_4 and the stack terminated in Co_3O_4. Each layer had an *equivalent thickness* of 25 nm and the total number of layers was 20.

The Ni thin film supported on carbon paper used as cathode was also prepared by MS-OAD, with the rotating plate described above. The target, a 50 mm diameter Ni disk (GoodFellow, 99.9%), was powered by a pulsed DC supply working at 150 W and a frequency of 120 kHz. The base pressure of the system was $2 \cdot 10^{-6}$ mbar and the deposition pressure was $5 \cdot 10^{-3}$ mbar. The deposition rate was 25 nm min^{-1} and the plasma gas was pure Ar dosed with a mass flow controller set at 30 sccm.

2.2. Characterization of the anodic thin film catalysts.

The microstructures of the films deposited on carbon paper and silicon substrates were examined by scanning electron microscopy (SEM) in planar view and cross sectional configurations with a Hitachi S4800 field emission microscope operated at 2 keV. Energy-Dispersive X-ray spectroscopy (EDX) analysis was carried out with a Bruker X-Flash Detector 4010.

Surface chemistry and stoichiometry of the deposits on carbon paper were evaluated by X-Ray photoelectron spectroscopy (XPS) in a PHOIBOS-100 spectrometer working at 20 eV constant pass energy. Binding Energy scale of the

spectra was referenced to the C 1s signal of the spurious carbon taken at 284.5 eV. The X-radiation used to excite the samples was unmonochromatic Mg Kα (hυ=1253.6 eV). In order to determine the surface atomic Co/Cu ratios, linear type backgrounds were used to determine the areas under the $Cu2p_{3/2}$ and $Co2p_{3/2}$ photoemission peaks and, later on, these raw areas were corrected for the photoionization cross sections of each electronic level [21], the transmission function of the analyzer [22], and, finally, the escape depth of photoelectrons [23].

DC electrical measurements, performed at room temperature by the four-point probe technique in a square configuration, were carried out on samples deposited on fused silica. A Keithley 2635A equipment was used for these measurements.

Elemental composition, in-depth elemental distribution, and total metal loading of the films deposited on polished silicon wafers were evaluated by Rutherford Backscattering Spectrometry (RBS) with a tandem accelerator (CNA, Seville, Spain). A beam of alpha particles with 2.8 MeV of energy was used for the analysis. The backscattered particles were collected with a silicon particle detector, placed 165º off the beam direction.

Crystallinity and phase analysis were performed by X-Ray diffraction (XRD) in a Panalytical X'PERT PRO. The crystallization behaviour of the $Cu_xCo_{3-x}O_4$ films was followed in situ between room temperature and 600 ºC, at a heating rate of 5 ºC min^{-1}. Sample was kept for 2 hours at each recording temperature.

FT-IR spectra of the films deposited on intrinsic silicon substrates were recorded in transmission mode with a Nicolet 510 spectrometer.

2.3. Electrochemical characterization in half-cell configuration

Electrochemical experiments were carried out in a three-electrode glass cell (half-cell configuration). It consisted of a working anodic electrode (0.53 cm^2 of geometric area),

an Ag/AgCl reference electrode (KCl, 3M, Metrohm®) and a platinum foil (Metrohm®) as counter electrode. Prior to the tests, a N_2 gas flow was bubbled through the solution for longer than 20 minutes. The flow of N_2 was kept during the experiment.

Electrochemical measurements were carried out with an Autolab potentiostat/galvanostat (PGSTAT30-ECOCHEMIE). The OER was monitored, in a 1.0 M KOH-deionized water solution at room temperature, by cyclic voltammetry in the range 0-750 mV vs. Ag/AgCl electrode and at a scan rate of 20 mV s^{-1}. Accelerated life testing of selected materials was performed by repetitive cyclic voltammetry (200 cycles) at a scan rate of 50 mV s^{-1}.

2.4. Preparation of the membrane electrode assembly (MEA)

The MEA consisted of an anion exchange membrane (Fumapem FAA-3-50, Fuel Cell Store), the $Cu_xCo_{3-x}O_4$ (Cu/Co at. ratio of 1.8) thin film supported on carbon paper (TGP-H-90 from Fuel Cell Earth) working as anode and the Ni thin film supported on carbon paper working as cathode. The geometric area of the two electrodes was 6.25 cm^2 and the catalyst loading 0.18 mg cm^{-2} (0.5 μm *equivalent thickness*) for the anode and 0.4 mg cm^{-2} (1 μm *equivalent thickness*) for the cathode obtained by RBS. These values were confirmed by weighting the electrodes before and after deposition of the catalysts.

The Fumapem FAA-3-50 anion exchange membrane has a very low resistance that provides a good option for fuel cell, electrolyser and other electrochemical applications. It is a brownish-transparent foil (45-50 μm thick) of PET with Br^- ions. Prior to use, it was immersed in an aqueous solution of 1 M KOH for 24 hours at room temperature, to convert its bromide functional groups (Br^-) into OH^- groups. Then, the membrane rinsed with demineralised water (pH ~7.0) was ready-to-use [24]. The MEA was sandwiched by hot pressing between two pieces of a stainless steel frame. Temperature was

increased at steps, from room temperature to 120 ºC (i.e., 10 ºC steps from 20 to 80 ºC, followed by 5 ºC steps from 80 to 120 ºC) and the sample kept for 2 minutes at each intermediate temperature and, after reaching the maximum value of 120 ºC, pressure (1 metric ton) was applied for 3 minutes.

2.5. Electrochemical characterization in the AEMWE configuration

Water electrolysis experiments were also carried out in an AEMWE full-cell (see the scheme of the experimental set up in the supporting information (Figure S2)). Electrochemical measurements were done with an Autolab potentiostat/galvanostat (PGSTAT30-ECOCHEMIE) generator. The temperature of the cell was varied between 25 and 70ºC. Data were registered by gradually changing the polarization from 1.0 V to 2.2 V at a scan rate of 5 mV s^{-1} in a 1.0 M KOH solution. To demonstrate the stability of the cell, chronopotentiometric experiments were subsequently performed during 18 hours at 40ºC. Gas-volume measurements were carried to determine the hydrogen production rate during the water electrolysis. Data were cross-checked via Faraday's Law. KOH concentration in the anode and cathode chambers was changed to study the effect of electrolyte concentration. The possible use of tap water and milli-Q water as electrolytes was also investigated.

Electrochemical impedance spectroscopy (EIS) measurements were carried out at two potentials (1.7 and 2.0 V) with an impedance module of the Autolab potentiostat/galvanostat (PGSTAT30-ECOCHEMIE). The impedance spectrum was collected in a frequency range from 10 kHz to 10 mHz and 10 mV as potential amplitude. These experiments were performed at 40ºC in a 1.0 M KOH solution.

3. Results and discussion

3.1. Physicochemical Characterization of $Cu_xCo_{3-x}O_4$ thin films and anodes

Several techniques were used to characterise the anodic $Cu_xCo_{3-x}O_4$ catalyst films. Specimens have been labelled as YY-CuCoO, where YY refers to the Co/Cu atomic ratio obtained by EDX analysis of samples prepared on carbon paper. For the different batches of anodic thin films, Table 1 shows the experimental parameters used for their synthesis (i.e., the power applied to the magnetron heads), the Co/Cu atomic ratios determined from either EDX or XPS analysis, the *equivalent thickness* determined by SEM, the total metal atom load (number of atoms per cm^{-2}) determined by RBS and the DC films electrical resistivity. The catalyst load, expressed in mg cm^{-2}, was calculated from the number of atoms per cm^2 obtained by RBS. Data in this table show that the Co/Cu atomic ratio in the films varies with the ratio of powers applied to the copper and cobalt targets during the co-deposition process. The mismatch in Co/Cu atomic ratio obtained with XPS and EDX might be attributed to the different probing depths of these techniques (XPS analyses just the upmost ~3 nm zone, while EDX analyses the whole film thickness). The films electrical properties varied also with their composition: the single oxide films present the highest resistance values and for the $Cu_xCo_{3-x}O_4$ thin films, this parameter decreases continuously with the Cu/Co atomic ratio. This tendency agrees with previous studies evidencing that the addition of Cu to $Cu_xCo_{3-x}O_4$ improves its electrical conductivity [25], while pure Co_3O_4 and CuO behave as semiconductor materials and have relatively higher electrical resistance. From the point of view of the use of these thin films as anodes, these low resistance values support that the electrochemical performance will not be significantly affected by high electrode impedances [25]. It is noteworthy that the films *equivalent thickness*, their atom density per unit surface and the metal load are very similar for all investigated electrodes, which

evidences an accurate control of the MS deposition process and supports that electrochemical results can be properly compared. It should be mentioned that the total metal load and atomic ratio distribution were homogeneous through the whole deposition area, the former is much lower than in powder based OER electrodes [2, 7, 26]. As an example, see the elemental mappings obtained for sample 1.8-CuCoO in Figure S3 of the supporting information.

Table 1. *Summary of the physicochemical characterization of the prepared anodic catalysts*.

Sample label	**Power (W_{Co}/W_{Cu})**	**Co/Cu at. ratio**		**Thickness (SEM) (nm)**	**Catalyst Load (RBS)**		**DC Resistance (Ω)**
		EDX	**XPS**		**Metal content (at cm^{-2})**	**Metal content (mg cm^{-2})**	
Co_3O_4	150/0	-	-	450	$4.05 \cdot 10^{18}$	0.20	$1.3 \cdot 10^{-2}$
16-CuCoO	150/50	16	9.7	454	$3.79 \cdot 10^{18}$	0.19	$3.0 \cdot 10^{-4}$
3.4-CuCoO	150/100	3.4	1.6	488	$3.83 \cdot 10^{18}$	0.19	$1.6 \cdot 10^{-4}$
1.8-CuCoO	150/150	1.8	1.0	441	$3.40 \cdot 10^{18}$	0.18	$2.3 \cdot 10^{-6}$
1.4-CuCoO	150/200	1.4	0.8	438	$3.75 \cdot 10^{18}$	0.21	$7.6 \cdot 10^{-7}$
CuO	0/150	0	0	469	$3.00 \cdot 10^{18}$	0.18	$8.7 \cdot 10^{-2}$

Figure 1 shows selected SEM images of 1.8-CuCoO films deposited on polished silicon wafer and carbon paper substrates. The cross section and normal SEM micrographs in Figures 1a) and 1b) reveal that the film deposited on silicon is formed by vertically aligned nanocolumns, which is the typical microstructure of OAD thin films [17, 27, 28]. The open porosity of these films supports their use as electrodes, where a high surface area in contact with the medium is a key requirement. When deposited on carbon paper, the film material grows only onto the most external fibres of the substrate (c.f Figure 1c)), but it still keep a high porosity, as revealed by the high magnification

image in Figure 1d) where agglomerated grains corresponding to the tips of the nanocolumns can be appreciated. It is expected that decoration of the outer fibres of the carbon paper substrates with these tiny aggregates provides a high electrochemical active surface area [24]. Composition was homogenous in all deposited zones, not only laterally, but also in the first and second layer of fibres, as evidenced by EDX mapping of the electrode surfaces (see supporting information Figure S3).

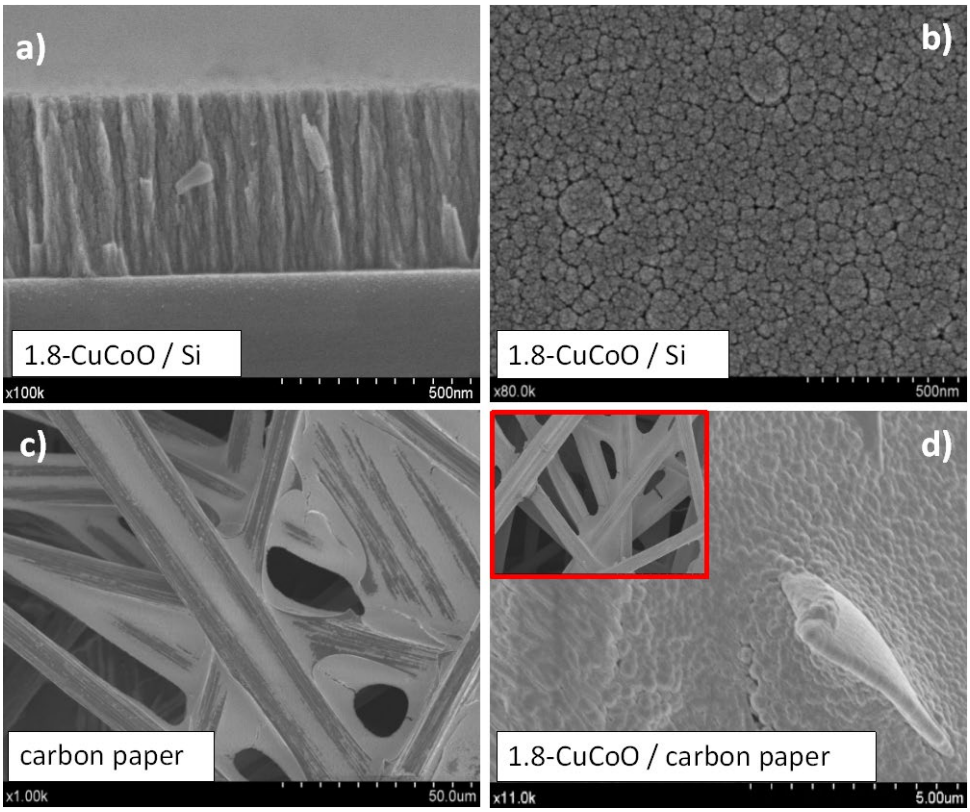

Figure 1. *SEM images of: a) 1.8-CuCoO sample supported on silicon substrate in a cross-sectional configuration; b) 1.8-CuCoO sample supported on silicon in planar view; c) bare carbon paper and d) 1.8-CuCoO sample supported on carbon paper in planar view. The inset shows the same sample with a different scale.*

Chemical state of catalyst films was typical of copper and cobalt oxides, as determined by XPS and FTIR. Figure 2 presents the Cu $2p_{3/2}$ and Co 2p photoelectron spectra recorded for the studied samples "as prepared". The binding energy of the Cu $2p_{3/2}$ peak at 934.0 eV and the strong satellite at 940-944 eV confirm that copper is in the form of

Cu^{2+} [29]. Meanwhile, the overall Co 2p peak shape and Co $2p_{3/2}$ binding energy at approximately 780 eV are typical of Co^{n+} (n=2,3) in Co_3O_4 [25, 30-32]. This assignment was confirmed by the FTIR analysis, that depicted spectra where Co^{3+}-$O^{=}$ and Cu^{2+}-$O^{=}$ characteristic bands [33-35] are clearly identified (see supporting information, Figure S4 and comments for further details). In addition, indirect evidences gained by XRD and the electrochemical behaviour of the multilayer $(CuO/Co_3O_4)^{10}$ electrodes (see below) sustain that, in the "as prepared" YY-CuCoO samples, copper and cobalt oxides are mixed in a common amorphous lattice (i.e., in the form of a $Cu_xCo_{3-x}O_4$ mixed oxide network).

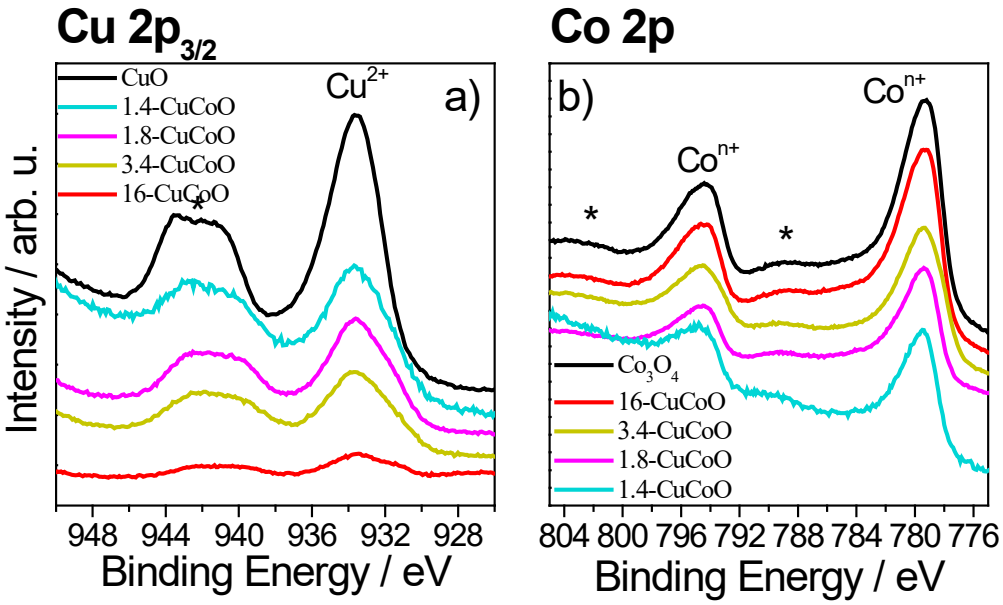

Figure 2. *XPS spectra of a) Cu $2p_{3/2}$ and b) Co 2p for YY-CuCoO samples supported on carbon paper. * denotes so-called satellite peaks which are typical of the Co^{3+} and Cu^{2+} oxidation states.*

3.2. Influence of the Co/Cu atomic ratio onto the OER

To retrieve information about the influence of the copper/cobalt atomic ratio in the OER, preliminary electrochemical analysis was carried out in the three-electrode glass cell (i.e., half-cell configuration) with the YY-CuCoO anodic catalysts deposited on

carbon paper substrates. Figure 3a) shows cyclic voltammetry diagrams as a function of the Co/Cu atomic ratio. In some voltammetry curves, such as in the case of pure Co_3O_4 sample, a small anodic feature at approximately 500 mV has been attributed to the Co(III)/Co(IV) redox couple [36, 37]. In addition, the corresponding cathodic peaks in the potential about 400-200 mV obtained on the reverse scan are due to Co(IV)/Co(III) redox reactions [5, 7, 36]. The onset potential for the OER was found between 500 and 600 mV, similar to that found for other copper and cobalt oxides systems prepared by alternative routes [5, 7, 38]. From the set of studied $Cu_xCo_{3-x}O_4$ thin films, sample 1.8-CuCoO rendered the highest current density and therefore the fastest OER kinetics within the explored potential range. A bulk Co/Cu ratio of 1.8 is within the optimal compositions reported in literature for Cu-cobaltite electrodes [5, 25, 29, 36]. However, surface Co/Cu ratio in this sample is close to 1 (see XPS value in Table 1) which suggests a preferential surface segregation of copper and that a particular local chemical environment around the Cu and Co sites yield a maximum catalytic activity.

Long-term stability under operation conditions of sample 1.8-CuCoO was proved by an accelerated life testing of repetitive cyclic voltammetry (200 cycles). The comparison in Figure 3b) of the 1st and 200th cycle reveals no distinctive difference after the accelerated aging test and supports that, despite their amorphous character, the MS-OAD Cu-cobaltite thin films exhibit a satisfactory long term stability as OER electrocatalysts. This behaviour is similar to that found for crystalline Cu-cobaltite anodic catalysts prepared by thermal decomposition of precursors [5, 13].

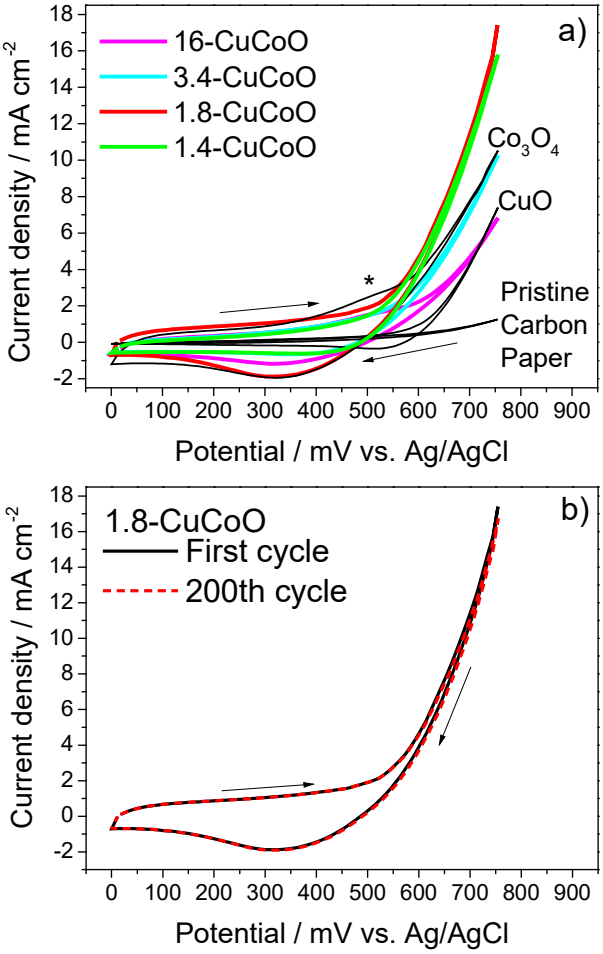

Figure 3. *a) Cyclic voltammograms of YY-CuCoO samples supported on carbon paper (* denotes Co(II)/Co(III) redox couple) and b) comparison of the first and 200th voltammogram cycle of 1.8-CuCoO sample at room temperature, with scan rate 20 mV·s^{-1} in 1.0 M KOH solution.*

To further investigate the surface properties of the 1.8-CuCoO electrodes after this accelerated aging test, used electrocatalyst samples were analysed by XPS. Surprisingly, the Co/Cu atomic ratio had changed to ca. 2.2, i.e., doubling the Co/Cu ratio of the "as prepared" sample, c.f., Table 1. A similar change occurred when the samples were just immersed in the KOH solution for a time period equivalent to that of the electrocatalytic tests. The shapes of the Cu 2p nor the Co 2p photoemission spectra did not vary after these liquid immersion tests and only differences were found in the O 1s region with the

appearance of a prominent peak at 531.0 eV attributed to a surface enrichment in OH-groups [33, 39, 40] (see spectra in the Figure S5). We attribute the observed change in Co/Cu surface ratio to some atom surface redistribution/segregation and/or to some preferential leaching into the electrolyte solution rather than to any selective delamination of the deposited anodic catalyst after the aging process. This is justified because the fluorine content (due to the Teflon coating of the fibers in the carbon paper [39, 41]) detected by XPS did not vary significantly after immersion. Thus, the Co/Cu ratio of 2.2 measured for the used samples supports that the most active surface electrocatalytic sites may consist of a three cations bonding arrangements of the type Co(O)Cu(O)Co rather than the binary Cu(O)Co bonding structure suggested by the XPS surface analysis of the pristine sample. This point deserves further confirmation by local order studies around the Cu and Co sites.

The higher efficiency of catalytic sites involving neighboring Co^{n+} and Cu^{2+} cations was further demonstrated by an experiment with the $(CuO/Co_3O_4)^{10}$ multilayer electrode, where copper and cobalt are separately distributed in a multilayer stack. The maximum current density found in this case was half that obtained for sample 1.8-CuCoO (see Figure S6 in the supporting information), in line with our proposal that most efficient electrocatalytic sites are formed by local arrangements of Cu and Co atoms.

3.3. Influence of crystallinity on the OER

The $Cu_xCo_{3-x}O_4$ thin films prepared by MS-OAD at room temperature were amorphous, a feature that contrasts with the crystalline character of equivalent electrocatalysts reported in literature prepared by thermal decomposition of precursor solutions [7, 14, 26]. To assess the influence of the electrode crystalline structure of the electrodes on the OER, we have studied the crystallization behaviour of the as prepared samples upon annealing in air at increasing temperatures. Figure 4 shows X-Ray Diffraction (XRD) diagrams of the 1.8-CuCoO sample deposited on carbon paper measured after its annealing at increasing temperatures. No well-defined diffraction peaks due to crystalline phases were detected for annealing temperatures below 400 ºC. This result confirms that the deposited electrodes, formed by a random solid solution of the Cu^{2+}, and Co^{n+} cations, are amorphous and do not present long range order in their structure. At temperatures above 450 ºC, diffraction peaks of CuO and $Cu_{0.7}Co_{2.3}O_4$ phases start to develop and they become clearly observed at higher temperatures [1, 29]. The presence of some minor Co_3O_4 contribution cannot be discharged. The formation of CuO crystallites indicates that the observed phase separation process will significantly alter the average distribution of atoms at the electrocatalyst surface, at least for the grains of the pure oxides. This effect, together with the possible sintering processes occurring at high temperature, suggests that the OER activity might be modified after electrode annealing. This point was checked by measuring the electrochemical performance of a 1.8-CuCoO film supported on two different substrates, carbon paper and Indium Tin Oxide (ITO), after heating these samples for two hours at 500º C. To control any possible secondary effect resulting from substrate heating, these ones were heated at 500 ºC before the deposition of the amorphous anodic film. Electrocatalytic

OER activities of these systems were examined by cyclic voltammetry in the half cell configuration.

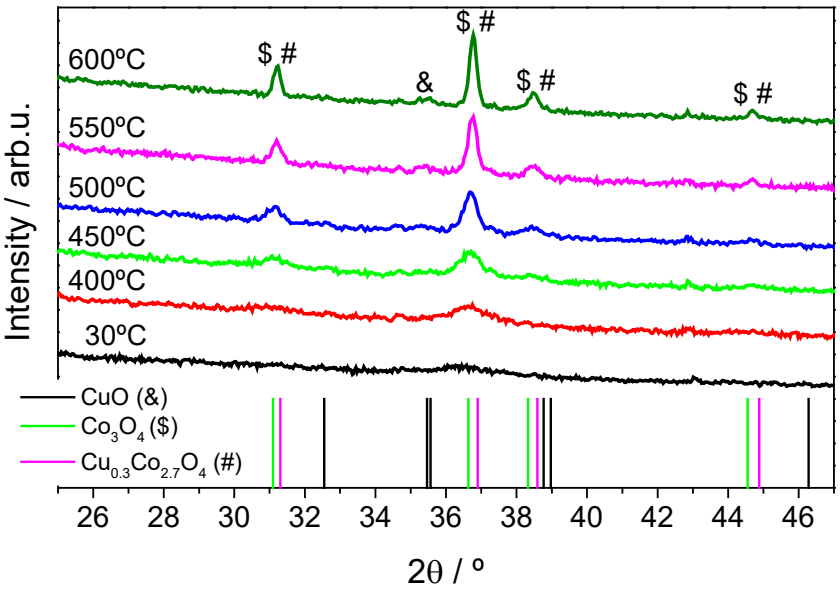

Figure 4. *X-Ray patterns of 1.8-CuCoO sample annealed at increasing temperatures. More significant diffraction lines of CuO (ref: 01-080-1268), Co_3O_4 (ref. 01-080-1535), and $Cu_{0.3}Co_{2.7}O_4$ (ref: 00-025-0270) phases are included.*

Figure 5a) and Figure 5b) shows the voltammograms obtained for as deposited and 500ºC annealed samples deposited on carbon paper and ITO substrates, respectively. The higher electrocatalytic activity found with carbon paper can be attributed to the higher electrical conductivity and easier electrolyte accessibility in this substrate. However, in the two cases, the electrocatalytic activity decreased after annealing at 500 ºC, thus supporting our considerations about the nature of the most efficient catalyst sites and/or pointing out a possible detrimental effect due to sintering [36]. From a practical point of view, these results disregard the need of any annealing treatment when using MS-OAD thin films as electrodes, thus simplifying their manufacturing procedure.

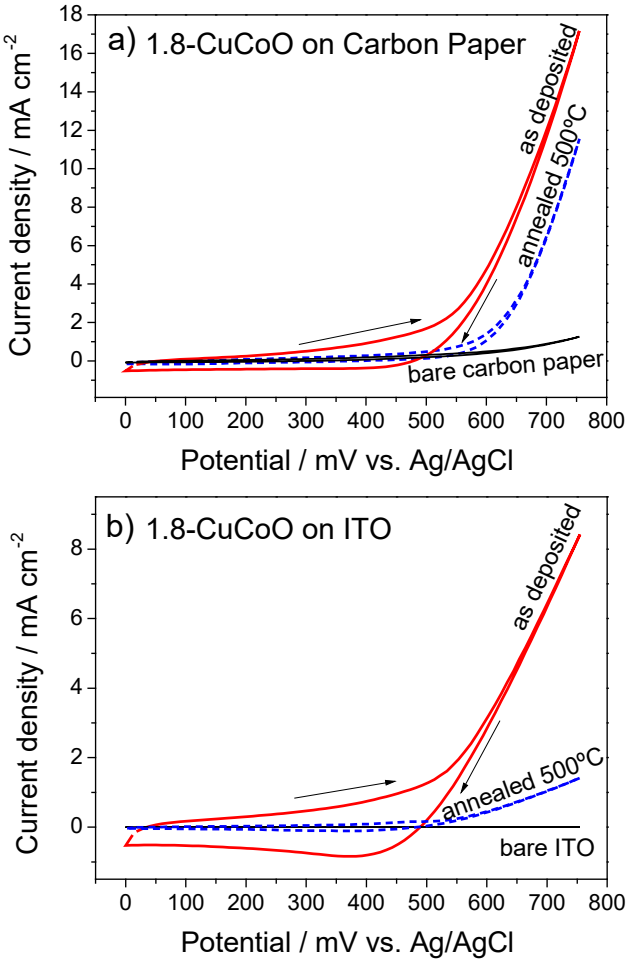

Figure 5. *Cyclic voltammograms of as deposited and crystallized 1.8-CuCoO sample supported on a) carbon paper and b) ITO evaluated with scan rate 20 mV* s^{-1} *in 1.0 M KOH solution at room temperature.*

3.4. Scale-up to AEMWE cell

To test the performance of the $Cu_xCo_{3-x}O_4$ anodic thin films under real operation conditions, experiments were carried out with the 1.8-CuCoO electrode integrated in a single electrolysis cell, provided with an anion exchange membrane in a MEA configuration and Ni thin film (see experimental section) acting as cathode. The linear voltammetry curves in Figure 6a) were obtained at several temperatures with 1.0 M KOH solution, while in Figure 6b) the curves correspond to various electrolyte solutions

at 40 ºC. In good agreement with other studies [7], recorded density curves show that a first activation exponential region is triggered at a potential threshold around 1.5 V (see Figure 6a) and then is followed by a lineal ohmic region, for current densities higher than 30 mA cm^{-2}. As expected, at constant intensity, cell potential decreased with increasing temperature due to an increase in both: the hydroxyl ion conductivity through the membrane and in the rate of catalytic hydrogen and oxygen evolution [42]. It can be also observed in Figure 6a that the electrolysis onset potential slightly decreases from 1.60 V at 25 ºC to 1.56 V at 70 ºC. The highest cell performance was found at 70 ºC, when it reached a current density of 110 mA cm^{-2} at 2.2 V. It is worth stressing that this value is close to that reported in literature for highly performance cells and electrodes incorporating anion exchange membranes (AEM) and much higher catalyst loads [26, 38].

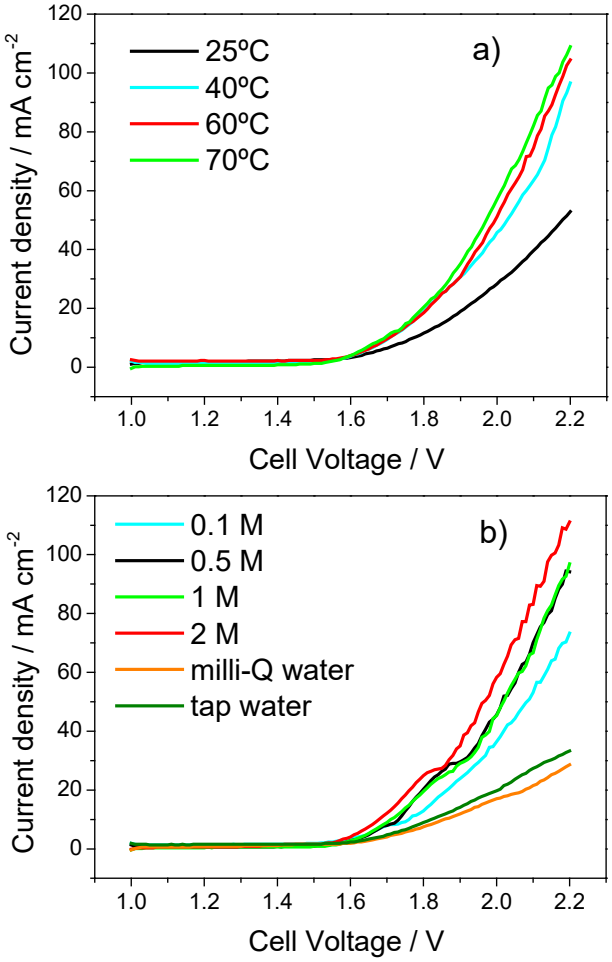

Figure 6. *Influence of a) the temperature (1.0 M KOH solution at temperature of 25, 40, 60, 70 ºC) and b) the electrolyte (at 40 ºC using different KOH concentration and water) on the polarization curves of the MEA prepared with a 1.8-CuCoO catalyst supported on carbon paper.*

Figure 6b) also shows that an increase in KOH concentration enhances the electrolyser performance, an effect that can be attributed to both an increase in ion conductivity through the membrane and in the anode electrocatalyst activity at higher pH values [14]. This behavior agrees with previous results reporting a lower internal resistance of the cells at higher pHs [6, 8, 42, 43]. A significant influence of ion conductivity in the experiments in Figure 6b) can be traced from the decrease in onset potential from 1.65 V for deionized water to 1.55 V for 2.0 M KOH solution, and by the fact that the

lowest electrocatalyic performance was obtained with pure deionized water (pH=6.0) and, therefore, a negligible concentration of OH^- ions.

As part of this analysis of the MEA, experiments similar to those in Figure 6 carried out with annealed anode films (at 500 ºC) revealed a clear decrease in performance in this case (see the i-V curves as a function of temperature and electrolyte type in supporting information, Figure S7). This behavior confirmed the results in Figure 5 about the deleterious effect on catalytic performance of segregation and/or crystallization processes occurring during heating. A decrease in performance could be also consistent to the observed EIS analysis carried out with the MEA incorporating either as deposited or annealed anodes (see the corresponding Nyquist plots shown in Figure S8 and the ohmic resistance values in Table S1 derived according to the equivalent RC circuit included as an inset in the figure [44, 45]. Thus, the anodic charge transfer resistance [44, 45] of the annealed anode at 1.7 V was higher than that of the as deposited anode (3.0 Ω vs 1.89 Ω, see table S1), which justify the observed lower OER performance of the annealed anode.

Stability tests were also carried out with the MEA at an intermediate electrolyte concentration of 1.0 M and 40ºC to avoid a too corrosive environment [46]. Under these conditions, the V-t plot in Figure 7 shows the stability of the cell during 18 hours operation at 25 mA cm^{-2} constant current. The curve depicts a sharp voltage increase at the beginning of the experiment that is followed by a rather constant voltage at the end of the experiment [9, 47]. Since the generated volume of hydrogen as a function of time followed the linear tendency predicted by the Faraday law (see inset in Figure 7, corresponding to the H_2 evolution during the first 30 minutes of operation), and a longer stability of the anode was proved by the three-electrode glass cell experiments (Figure 3b), we attribute the observed slight deactivation with time to a certain degradation of

the membrane (e.g., affecting the polymer backbone or the ion exchange groups). Nonetheless, the hydrogen energy production yield of 51 kW $(KgH_2)^{-1}$ determined in this experiment is similar to other values obtained with AEM electrolysers and conventional electrode materials [6].

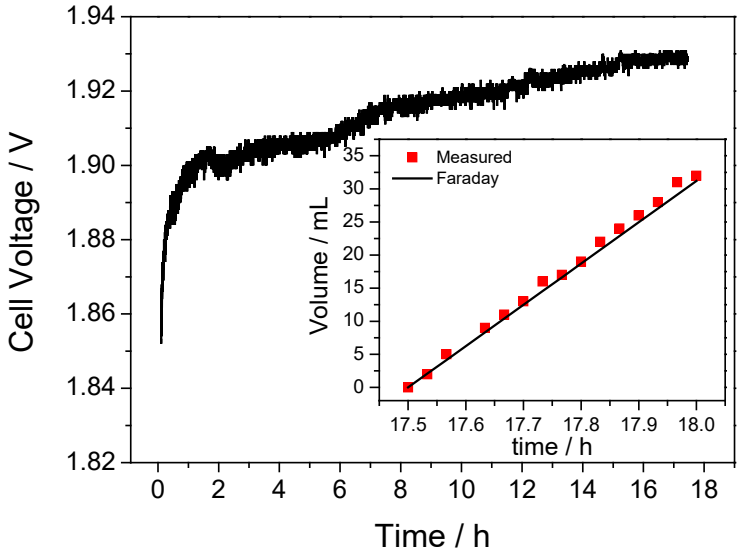

Figure 7. *Chronopotentiometry experiment using a constant current density of 25 mA* cm^{-2} *at 40 ºC in a 1.0 M KOH solution. Inset: comparison of the measured and Faradaic hydrogen production.*

To put in context the MEA performance herein obtained, Table 2 summarizes a series of published AEM electrolysis results carried out with similar catalysts and working conditions, except for the use of different ionomers (ionomers are compounds used to enhance electrolysis performance by creating transport pathways between membrane and reaction sites [2, 6]). Although the absolute electrocatalytic activity of our system is lower than that reported in these MEAs studies (for example in ref. [5] using 3 mg cm^{-2} $Cu_xCo_{3-x}O_4$ well-crystallized nanoparticles as anode and 1 mg Pt cm^{-2} as cathode they obtained 1000 mA cm^2 at 1.8 V), the extremely low amount of metal loading in our systems makes them the most efficient in terms catalyst load. This high performance might be due to particular mesoporous microstructure of the deposited catalysts by MS-

OAD. An additional advantage in terms of costs is the use of low load of Ni cathode catalyst, also prepared at room temperature by MS. Finally, also mention that the cost associated with the traditional annealing processes needed to obtain a well crystallize mixed cobaltite catalysts is also removed.

Table 2. *Comparison of our results with previous studies using milli-Q water as anodic feeding stream.*

Anode	**Membrane**	**Cathode**	**Ionomer**	**Normalized Current at 2 V with mili-Q water (mA/mg)**	**Temperature (ºC)**	**References**
Co_3O_4-CuO	Fumapem FAA-3-50	Ni	No	92.11	40	This study
$Cu_{0.7}Co_{2.3}O_4$	mm-qPVBz/Cl-	Ni	YES	25.00	40	[22]
CuCoOx	Tokuyama A-201	Ni/(CeO_2-La_2O_3)/C	YES	11.67	60	[2]
CuCoOx	QAPPO membrane	Ni/(CeO_2-La_2O_3)/C	YES	74.00	60	[48]
$Cu_{0.7}Co_{2.3}O_4$	Prepared	Pt	YES	73.33	25	[5]
$Cu_xMg_{0.9-x}Co_{2.1}O_4$	Prepared	Pt	YES	66.67	40	[34]
$Cu_{0.7}Co_{2.3}O_4$	Cranfield-membrane	Ni	YES	50.00	25	[49]

4. Conclusions

The obtained results have demonstrated for the first time that active and stable $Cu_xCo_{3-x}O_4$ ultrathin electrodes can be prepared by MS-OAD at room temperature for their use in AEMWE cells. In fact, the normalized electrocatalytic activity per mass of metal load for the most active catalysts formulation reported here exceeds the values obtained for

similar electrocatalyst systems in literature. From a fundamental point of view, the electrochemical performance of the as deposited electrodes, together with the characterization of the used catalyst surfaces suggest that local arrangements combining one Cu and two Co cations constitute surface sites providing a maximum catalytic activity for the OER. Although further studies are still required to make the overall current values competitive with others reported in the literature, the obtained results prove the feasibility of this preparation technique for OER catalyst fabrication and the development of cheap and reliable electrolysis devices. The long term stability tests carried out in a three electrode cell system and the MEA device confirm the suitability of this ultra-thin electrocatalysts for practical applications and support the use of MS-OAD for large area electrode fabrication.

Acknowledgments

Authors thank the European Regional Development Funds program (EU-FEDER), the MINECO-AEI (201560E055, MAT2016-79866-R and network MAT2015-69035-REDC) and the MECD (grant FPU17/00344) for financial support.

REFERENCES

[1] K.E. Kang, C.H. Kim, M.S. Lee, C.W. Jung, Y.D. Kim, J.H. Lee, Stability of a Cu0.7Co2.3O4 electrode during the oxygen evolution reaction for alkaline anion-exchange membrane water electrolysis, Journal of the Korean Physical Society, 72 (2018) 52-56.

[2] I. Vincent, A. Kruger, D. Bessarabov, Development of efficient membrane electrode assembly for low cost hydrogen production by anion exchange membrane electrolysis, International Journal of Hydrogen Energy, 42 (2017) 10752-10761.

[3] S.H. Ahn, B.-S. Lee, I. Choi, S.J. Yoo, H.-J. Kim, E. Cho, D. Henkensmeier, S.W. Nam, S.-K. Kim, J.H. Jang, Development of a membrane electrode assembly for alkaline water electrolysis by direct electrodeposition of nickel on carbon papers, Applied Catalysis B: Environmental, 154-155 (2014) 197-205.

[4] Y. Leng, G. Chen, A.J. Mendoza, T.B. Tighe, M.A. Hickner, C.Y. Wang, Solid-state water electrolysis with an alkaline membrane, Journal of the American Chemical Society, 134 (2012) 9054-9057.

[5] X. Wu, K. Scott, CuxCo3-xO4 (0 [less-than-or-equal] x < 1) nanoparticles for oxygen evolution in high performance alkaline exchange membrane water electrolysers, Journal of Materials Chemistry, 21 (2011) 12344-12351.

[6] I. Vincent, D. Bessarabov, Low cost hydrogen production by anion exchange membrane electrolysis: A review, Renewable and Sustainable Energy Reviews, 81 (2018) 1690-1704.

[7] X. Wu, K. Scott, A Li-doped Co<inf>3</inf>O<inf>4</inf>oxygen evolution catalyst for non-precious metal alkaline anion exchange membrane water electrolysers, International Journal of Hydrogen Energy, 38 (2013) 3123-3129.

[8] L. Zeng, T.S. Zhao, Integrated inorganic membrane electrode assembly with layered double hydroxides as ionic conductors for anion exchange membrane water electrolysis, Nano Energy, 11 (2015) 110-118.

[9] M.K. Cho, A. Lim, S.Y. Lee, H.J. Kim, S.J. Yoo, Y.E. Sung, H.S. Park, J.H. Jang, A review on membranes and catalysts for anion exchange membrane water electrolysis single cells, Journal of Electrochemical Science and Technology, 8 (2017) 183-196.

[10] E. Rasten, G. Hagen, R. Tunold, Electrocatalysis in water electrolysis with solid polymer electrolyte, Electrochimica Acta, 48 (2003) 3945-3952.

[11] M. Hamdani, R.N. Singh, P. Chartier, Co3O4 and co-based spinel oxides bifunctional oxygen electrodes, International Journal of Electrochemical Science, 5 (2010) 556-577.

[12] I. Nikolov, R. Darkaoui, E. Zhecheva, R. Stoyanova, N. Dimitrov, T. Vitanov, Electrocatalytic activity of spinel related cobaltites MxCo3-xO4 (M = Li, Ni, Cu) in the oxygen evolution reaction, Journal of Electroanalytical Chemistry, 429 (1997) 157-168.

[13] A.B. Calcerrada, A.R. de la Osa, H.A.E. Dole, F. Dorado, E.A. Baranova, A. de Lucas-Consuegra, Stability Testing of Pt x Sn1 − x /C Anodic Catalyst for Renewable Hydrogen Production Via Electrochemical Reforming of Ethanol, Electrocatalysis, 9 (2018) 293-301.

[14] G. Gupta, K. Scott, M. Mamlouk, Performance of polyethylene based radiation grafted anion exchange membrane with polystyrene-b-poly (ethylene/butylene)-b-polystyrene based ionomer using NiCo2O4 catalyst for water electrolysis, Journal of Power Sources, 375 (2018) 387-396.

[15] A. Barranco, A. Borras, A.R. Gonzalez-Elipe, A. Palmero, Perspectives on oblique angle deposition of thin films: From fundamentals to devices, Progress in Materials Science, 76 (2016) 59-153.

[16] J.P. Biethan, D. Arhilger, J. Pistner, H. Reus, M. Stapp, H. Hagedorn, High precision optical filter based on magnetron sputtering: Direct coating on glass and silicon wafers, Vakuum in Forschung und Praxis, 29 (2017) 26-31.

[17] J. Gil-Rostra, F. García-García, F. Yubero, A.R. González-Elipe, Tuning the transmittance and the electrochromic behavior of CoxSiyOz thin films prepared by magnetron sputtering at glancing angle, Solar Energy Materials and Solar Cells, 123 (2014) 130-138.

[18] J. Gil-Rostra, M. Cano, J.M. Pedrosa, F.J. Ferrer, F. García-García, F. Yubero, A.R. González-Elipe, Electrochromic Behavior of WxSiyOz Thin Films Prepared by Reactive Magnetron Sputtering at Normal and Glancing Angles, ACS Applied Materials & Interfaces, 4 (2012) 628-638.

[19] J. Gil-Rostra, F.J. García-García, F.J. Ferrer, A.R. González-Elipe, F. Yubero, Microstructure of mixed oxide thin films prepared by magnetron sputtering at oblique angles, Thin Solid Films, 591 (2015) 330-335.

[20] R. Alvarez, J.-M. Garcia-Martin, C. Lopez-Santos, V. Rico, F.J. Ferrer, J. Cotrino, A. Gonzalez-Elipe, A. Palmero, On the Deposition Rates of Magnetron Sputtered Thin Films at Oblique Angles, 2014.

[21] J.H. Scofield, Hartree-Slater subshell photoionization cross-sections at 1254 and 1487 eV, Journal of Electron Spectroscopy and Related Phenomena, 8 (1976) 129-137.

[22] D. Briggs, Seah, M.P., Practical Surface Analysis by Auger and X-Ray Photoelectron Spectroscopy, 1983.

[23] S. Tanuma, C.J. Powell, D.R. Penn, Calculations of electron inelastic mean free paths. IX. Data for 41 elemental solids over the 50 eV to 30 keV range, Surface and Interface Analysis, 43 (2011) 689-713.

[24] A. de Lucas-Consuegra, A.R. de la Osa, A.B. Calcerrada, J.J. Linares, D. Horwat, A novel sputtered Pd mesh architecture as an advanced electrocatalyst for highly efficient hydrogen production, Journal of Power Sources, 321 (2016) 248-256.

[25] J. Jia, X. Li, G. Chen, Stable spinel type cobalt and copper oxide electrodes for O<inf>2</inf>and H<inf>2</inf>evolutions in alkaline solution, Electrochimica Acta, 55 (2010) 8197-8206.

[26] Y.C. Cao, X. Wu, K. Scott, A quaternary ammonium grafted poly vinyl benzyl chloride membrane for alkaline anion exchange membrane water electrolysers with no-noble-metal catalysts, International Journal of Hydrogen Energy, 37 (2012) 9524-9528.

[27] P. Salazar, F.J. Garcia-Garcia, F. Yubero, J. Gil-Rostra, A.R. González-Elipe, Characterization and application of a new pH sensor based on magnetron sputtered porous WO<inf>3</inf>thin films deposited at oblique angles, Electrochimica Acta, 193 (2016) 24-31.

[28] F.J. Garcia-Garcia, P. Salazar, F. Yubero, A.R. González-Elipe, Non-enzymatic Glucose electrochemical sensor made of porous NiO thin films prepared by reactive magnetron sputtering at oblique angles, Electrochimica Acta, 201 (2016) 38-44.

[29] M. Polyakov, A.E. Surkus, A. Maljusch, S. Hoch, A. Martin, Impact of the Co : Cu Ratio in CoCu-Containing Oxidic Solids on their Activity for the Water-Splitting Reaction, ChemElectroChem, 4 (2017) 2109-2116.

[30] M.E.A. Warwick, G. Carraro, D. Barreca, A. Gasparotto, C. Maccato, TiO2-Fe2O3 and Co3O4-Fe2O3 nanocomposites analyzed by X-ray Photoelectron Spectroscopy, Surface Science Spectra, 22 (2015) 34-46.

[31] V.M. Jiménez, A. Fernández, J.P. Espinós, A.R. González-Elipe, The state of the oxygen at the surface of polycrystalline cobalt oxide, Journal of Electron Spectroscopy and Related Phenomena, 71 (1995) 61-71.

[32] J.P. Espinós, J. Morales, A. Barranco, A. Caballero, J.P. Holgado, A.R. González-Elipe, Interface Effects for Cu, CuO, and Cu2O Deposited on SiO2 and ZrO2. XPS Determination of the Valence State of Copper in Cu/SiO2 and Cu/ZrO2 Catalysts, The Journal of Physical Chemistry B, 106 (2002) 6921-6929.

[33] A. Shanmugavani, R.K. Selvan, Improved electrochemical performances of CuCo2O4/CuO nanocomposites for asymmetric supercapacitors, Electrochimica Acta, 188 (2016) 852-862.

[34] A. El-Trass, H. ElShamy, I. El-Mehasseb, M. El-Kemary, CuO nanoparticles: Synthesis, characterization, optical properties and interaction with amino acids, Applied Surface Science, 258 (2012) 2997-3001.

[35] L. Wei, X. Dong, M. Ma, Y. Lu, D. Wang, S. Zhang, D. Zhao, Q. Wang, Co3O4 hollow fiber: An efficient catalyst precursor for hydrolysis of sodium borohydride to generate hydrogen, International Journal of Hydrogen Energy, 43 (2018) 1529-1533.

[36] Q. Zhang, Z.D. Wei, C. Liu, X. Liu, X.Q. Qi, S.G. Chen, W. Ding, Y. Ma, F. Shi, Y.M. Zhou, Copper-doped cobalt oxide electrodes for oxygen evolution reaction prepared by magnetron sputtering, International Journal of Hydrogen Energy, 37 (2012) 822-830.

[37] B. Chi, H. Lin, J. Li, Cations distribution of Cu<inf>x</inf>Co<inf>3-x</inf>O<inf>4</inf>and its electrocatalytic activities for oxygen evolution reaction, International Journal of Hydrogen Energy, 33 (2008) 4763-4768.

[38] X. Wu, K. Scott, A non-precious metal bifunctional oxygen electrode for alkaline anion exchange membrane cells, Journal of Power Sources, 206 (2012) 14-19.

[39] X. Li, R. Ding, W. Shi, Q. Xu, D. Ying, Y. Huang, E. Liu, Hierarchical porous Co(OH)F/Ni(OH)2: A new hybrid for supercapacitors, Electrochimica Acta, 265 (2018) 455-473.

[40] H. Li, W. Hao, J. Hu, H. Wu, A photoelectrochemical sensor based on nickel hydroxyl-oxide modified n-silicon electrode for hydrogen peroxide detection in an alkaline solution, Biosensors and Bioelectronics, 47 (2013) 225-230.

[41] L. Zhu, Y. Zheng, T. Hao, X. Shi, Y. Chen, J. Ou-Yang, Synthesis of hierarchical ZnO nanobelts via Zn(OH)F intermediate using ionic liquid-assistant microwave irradiation method, Materials Letters, 63 (2009) 2405-2408.

[42] C.C. Pavel, F. Cecconi, C. Emiliani, S. Santiccioli, A. Scaffidi, S. Catanorchi, M. Comotti, Highly efficient platinum group metal free based membrane-electrode assembly for anion exchange membrane water electrolysis, Angewandte Chemie - International Edition, 53 (2014) 1378-1381.

[43] O.F. Selamet, F. Becerikli, M.D. Mat, Y. Kaplan, Development and testing of a highly efficient proton exchange membrane (PEM) electrolyzer stack, International Journal of Hydrogen Energy, 36 (2011) 11480-11487.

[44] N. Wagner, M. Schulze, Change of electrochemical impedance spectra during CO poisoning of the Pt and Pt–Ru anodes in a membrane fuel cell (PEFC), Electrochimica Acta, 48 (2003) 3899-3907.

[45] H. Ju, S. Giddey, S.P.S. Badwal, R.J. Mulder, Electro-catalytic conversion of ethanol in solid electrolyte cells for distributed hydrogen generation, Electrochimica Acta, 212 (2016) 744-757.

[46] A. Lim, M.K. Cho, S.Y. Lee, H.J. Kim, S.J. Yoo, Y.E. Sung, J.H. Jang, H.S. Park, A review of industrially developed components and operation conditions for anion exchange membrane water electrolysis, Journal of Electrochemical Science and Technology, 8 (2017) 265-273.

[47] P. Ganesan, A. Sivanantham, S. Shanmugam, Nanostructured Nickel-Cobalt-Titanium Alloy Grown on Titanium Substrate as Efficient Electrocatalyst for Alkaline Water Electrolysis, ACS Applied Materials and Interfaces, 9 (2017) 12416-12426.

[48] L. Zeng, T.S. Zhao, An effective strategy to increase hydroxide-ion conductivity through microphase separation induced by hydrophobic-side chains, Journal of Power Sources, 303 (2016) 354-362.

[49] X. Wu, K. Scott, A polymethacrylate-based quaternary ammonium OH− ionomer binder for non-precious metal alkaline anion exchange membrane water electrolysers, Journal of Power Sources, 214 (2012) 124-129.